

Uniform InGaAs quantum dot arrays fabricated using nanosphere lithography

X. Qian,^{a)} J. Li, D. Wasserman, and W. D. Goodhue

Department of Physics and Applied Physics, Photonics Center, University of Massachusetts Lowell, Massachusetts 01854, USA

(Received 9 September 2008; accepted 13 November 2008; published online 11 December 2008)

We demonstrate the fabrication of optically active uniform InGaAs quantum dot arrays by combining nanosphere lithography and bromine ion-beam-assisted etching on a single InGaAs/GaAs quantum well. A wide range of lateral dot sizes was achieved from an oxygen plasma nanosphere resizing process. The increased lateral confinement of carriers in the dots results in low temperature photoluminescence blueshifts from 0.5 to 11 meV. Additional quantization was achieved using a selective wet-etch process. Our model suggests the presence of a 70 nm dead layer in the outer InGaAs radial edge, which we believe to be a result of defects and dislocations introduced during the dry-etch process. © 2008 American Institute of Physics.

[DOI: [10.1063/1.3040683](https://doi.org/10.1063/1.3040683)]

Since the 1980s, significant effort has been devoted to the realization of uniform III-V semiconductor quantum dot (QD) structures able to provide three dimensional (3D) carrier confinement. The most frequently used techniques for fabrication or growth of In(Ga)As/Ga(Al)As QDs include lithography,¹ interface fluctuations,² self-assembly,^{3,4} and Ga droplet epitaxy.⁵ Of these methods, epitaxial growth of self-assembled QDs (SAQDs) is often favored for the fabrication of compact high speed optical devices such as lasers,⁶ emitters,⁷ and photodetectors,⁸ as these nanostructures can be grown pseudomorphically, resulting in fewer defects and dislocations than other QD fabrication techniques. However, because such QD growth is a self-assembly process, control of dot geometry and size uniformity is problematic.

Alternatively, nanolithography (NL)⁹⁻¹² allows the fabrication of QDs by patterning of quantum wells (QWs). Great strides have been made of late in NL techniques as a result of the ever-increasing need to reduce pattern feature sizes to the nanometer scale (<200 nm). The well-known top-down techniques in nanostructure patterning include advanced optical lithography,⁹ electron-beam lithography,¹⁰ x-ray lithography,¹¹ and ion-beam lithography.¹² However, the cost and complexity of these techniques increase dramatically with the need for reduced feature sizes over large areas. In addition, damage from the NL and nanopatterning processes often degrades the optical properties of the resulting nanostructures. Nanosphere lithography (NSL)¹³ is an inexpensive alternative nanofabrication technique to the aforementioned processes. Using a standard photoresist spinner and a properly prepared polymer nanosphere solution, a self-assembled, ordered, and close-packed sphere array can be formed on a semiconductor substrate and then used as the template or mask to transfer the nanosphere array pattern to the substrate. The sizes of nanospheres can be tuned from 20 to 1000 nm, offering a simple solution to scale nanostructure feature sizes. NSL is an inherently parallel and high throughput process. With improvements in the domain sizes of the self-assembled sphere arrays, NSL has great potential in fabricating optical devices,¹⁴ electronic devices,¹⁵ and

biosensors.¹⁶ Over the past decade, NSL has been used to nanopattern silicon and glass substrate surfaces.¹⁷ Recently, we demonstrated the realization of nanopillar and nanohole arrays on GaAs substrates using NSL.¹⁸ In this work, NSL is used to fabricate optically active highly uniform InGaAs QDs in a GaAs matrix.

Our initial QW sample consists of a 6 nm wide In_{0.2}Ga_{0.8}As/GaAs single QW (SQW) capped with a 50 nm GaAs layer, grown by a solid source Veeco Gen-II molecular beam epitaxy (MBE) system. The as-grown SQW sample was then spin coated with 350 nm diameter polystyrene nanospheres to form a single ordered and close-packed nanosphere array. O₂ plasma reactive ion etching (O₂ plasma RIE) was then used to etch the spheres, allowing postspin feature size control. By utilizing an identical etch recipe, but varying etch duration, a wide range of sphere sizes were achieved. Following the nanosphere deposition and subsequent resizing, a bromine ion-beam-assisted-etching (Br-IBAE) process, which has been shown to have a large selectivity in etching GaAs with a polystyrene mask, was used to etch through InGaAs QW layer using resized sphere array as a mask. The nanosphere array was then removed by means of a second O₂ plasma etch, leaving an array of highly uniform InGaAs QDs. The fabrication process is shown in Fig. 1(a) and each step is characterized using scanning electron microscopy (SEM), as shown in Fig. 1(b). The density of these triangular distributed QDs is determined by the original sphere size. When 350 nm diameter nanospheres were used, a QD density of approximately $1 \times 10^9 \text{ cm}^{-2}$ can be obtained, although higher dot densities are achievable with smaller diameter spheres.

The SEM images in Fig. 1(b) show high uniformity of QDs array obtained by the NSL process. Additionally, the high selectivity of the Br-IBAE process at elevated temperatures¹⁹ results in clean vertical nanopillars. The sizes of nanosphere mask and the resulting QDs were measured by SEM. During the O₂ plasma RIE nanosphere resizing step, the sizes of thinned nanosphere can be tuned by varying the etch time, micropower, and rf power. In this experiment, using an O₂ flow rate of 10 SCCM (SCCM denotes cubic centimeter per minute at STP), micropower of 100 W, and rf

^{a)}Electronic mail: xifeng_qian@student.uml.edu.

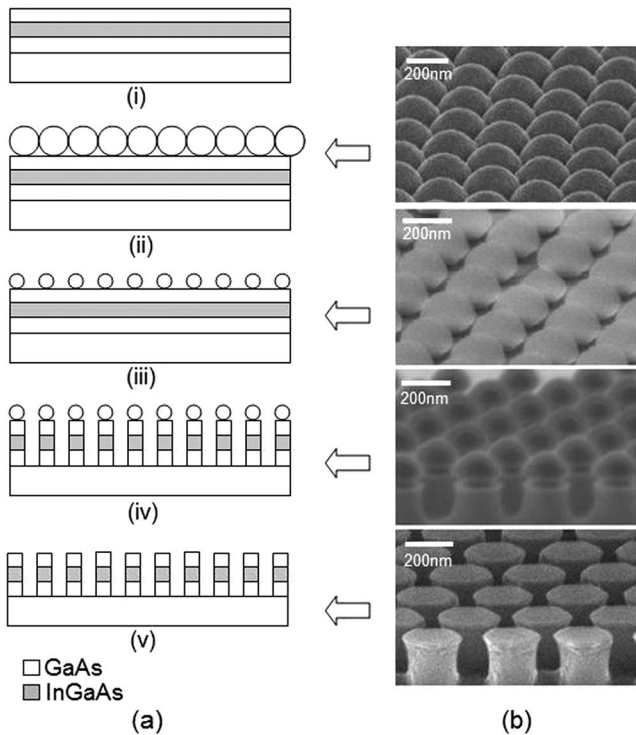


FIG. 1. Column (a) shows schematic illustrations of the fabrication process for InGaAs/GaAs QDs nanopillars; column (b) provides SEM images for each process step. (i) MBE grown InGaAs SQW structure. (ii) Nanosphere spin-on. (iii) Nanosphere resizing by O_2 plasma RIE. (iv) Etch of nanopillar vertical sidewalls by Br-IBAE. (v) Removal of resized nanospheres by O_2 plasma RIE, leaving uniform array of InGaAs cylindrical QDs.

power of 20 W, nanosphere sizes ranging from 275 to 170 nm were achieved by varying the etch time from 40 to 66 s.

Low temperature (77 K) photoluminescence (PL) of the fabricated QD samples was measured using a He-Ne laser as the exciting source and a Horiba Jobin-Yvon iHR320 spectrometer with a liquid nitrogen-cooled charge coupled device detector. Low temperature PL allows for a qualitative determination of the QD optical quality. In addition, the change in the PL peak position from the QDs, as compared to that from the original unprocessed SQW heterostructure, allows for the determination of the degree of quantization of carriers in the QDs. The PL energy shifts of QD samples with respect to the SQW sample are shown in Fig. 2. The energy blueshifts as a function of RIE etch time demonstrate the realization of quantization effects from lateral carrier confinement. Figure 2 also shows that the full width at half maximum (FWHM) of QW PL peak is 15 meV, while FWHM of QDs PL peaks are 9–12 meV. This spectral width narrowing of PL peak is believed to be a result of the QD delta functionlike distribution of density of states. However, a significant decrease in linewidth for the smaller diameter nanopillars was not observed when compared to the largest diameter nanopillar sample. We believe this can be explained by the increased effects of nanopillar size fluctuations on smaller diameter features, which has been observed in previous work.²⁰ In comparison with PL spectra from self-assembled InAs/GaAs QDs,²¹ which show a typical FWHM of 35 meV due to strong size nonuniformity, our NSL-fabricated QDs show narrower PL spectral widths, demonstrating improved size uniformity. An improved uniformity, when compared to SAQDs, is typical for NL-fabricated QDs.²² However, this

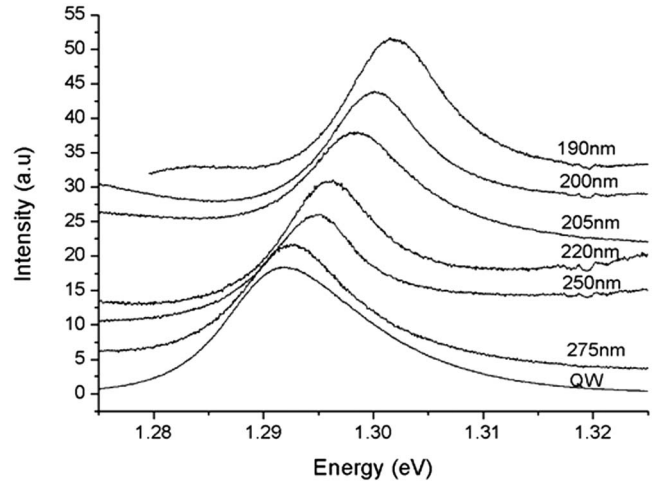


FIG. 2. PL spectra of SQW and QDs with various geometrical diameters obtained at 77 K with an excitation energy density of 100 W/cm^2 .

improvement is often offset by the degraded optical properties of the nanostructures resulting from the surface damage introduced by fabrication processes. In our samples, the high density plasma generated during both RIE and Br-IBAE processes can severely deteriorate the sphere morphology, damage the surface of GaAs, and therefore form an amorphized layer at the surface. This can result in the formation of an effective “dead layer,”²³ in which nonradiative recombination processes dominate. This dead layer will also reduce the effective size of the QDs, as carriers able to participate in optical processes are confined to the undamaged region of the QD. Typically, for semiconductor/air interfaces, Fermi level pinning by surface states results in the formation of a depletion layer below the interface.²⁴ However, in our structures the undamaged InGaAs material does not interface directly with air but instead sees the etch-damaged material. Fermi level pinning between high-quality InGaAs and etch-damaged InGaAs is less well understood and presumably will depend on the type of etch and the intensity of the reaction at etched surface. In order to estimate the magnitude of the etch damage introduced to the nanopillars, the transition energies between the 1e-1hh levels as a function of dot sizes have been calculated using a COMSOL simulation. Because the lateral confinement energies are assumed to be much smaller than the quantization energies in our quantum structures, we took the vertical and lateral quantizations as separable. In addition, we assumed a rectangular potential well in the growth direction, large potential barriers (resulting from the damaged InGaAs material) in the lateral direction, and standard InGaAs band structure data.²² Such a model, while inexact, provides a reasonably accurate picture of the device quantum structure and allows for an approximate estimate of the dead layer thickness in our nanopillars.

The result of our calculations, using the geometrical size of the nanopillars determined by SEM, is plotted as a solid line while the experimental data from the real samples are shown as diamonds in Fig. 3. There is a clear lateral offset between the experimental and simulated data. However, when a dead layer of 70 nm around the nanopillar is included in the model, reducing the QD effective size by 140 nm, the calculated spectral peak positions align very closely with the experimental data. The calculated peak shift as a function of nanopillar size, incorporating the dead layer, is shown in

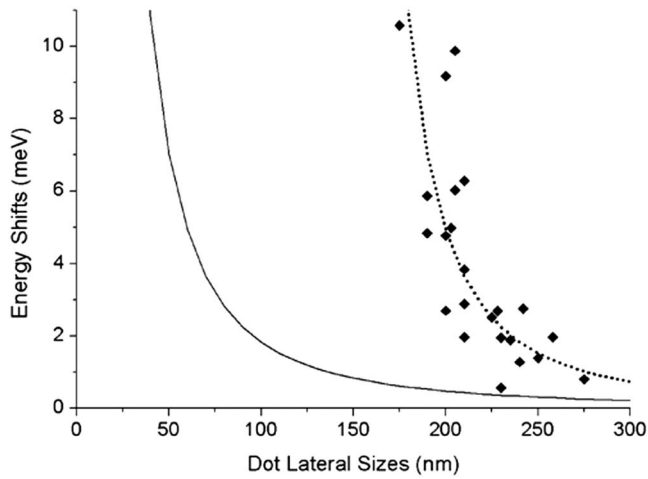


FIG. 3. Energy shift data of fabricated freestanding InGaAs/GaAs QDs as a function of dot diameters (diamonds), which are horizontally displaced from initial calculations using QD area equal to the nanopillar diameter (solid line), but agree well with the model calculation when taking 70 nm dead layer into account (dotted line).

Fig. 3 as a dotted line. This result suggests that the geometrical diameters of freestanding QDs are 140 nm larger than the effective lateral diameters, as a result of the 70 nm thick dead layer around the perimeter of the pillar.

The fabricated QD emission energy can be further tuned by means of an InGaAs-selective wet-etch process. Using a citric acid:H₂O₂ (2:1 by volume) etchant, we etched the thin InGaAs layer inward on 235 nm diameter InGaAs QDs. The geometry of the resulting 40 s etched QDs is shown in Fig. 4 (inset), which clearly show the decrease in the InGaAs QDs lateral size, resulting in an additional blueshift of the PL peak, as shown in Fig. 4. However, 60 nm diameter QDs, resulting from longer etch time, show no PL emission. Although wet chemical etching most likely produce no dead layers at the open sidewalls of the nanostructures, previous work has shown orders of magnitude reduction in the PL intensity from small dots compared to that from the large dots.²⁰ In the referenced work the authors attribute the loss of

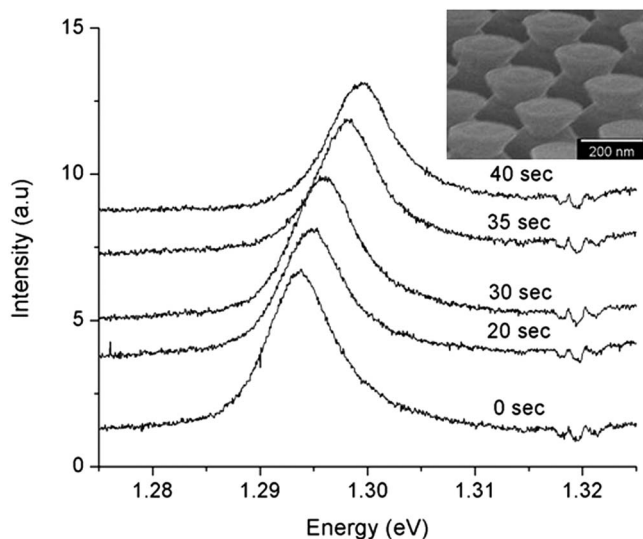


FIG. 4. SEM of lateral etched InGaAs QDs (inset) with 40 s lateral wet-etch showing approximately 150 nm diameter. Low temperature PL data from the lateral etched QDs demonstrate an additional energy blueshift by means of the selective InGaAs etch.

PL intensity to nonradiative carrier recombination at the open sidewalls for small dots. If a similar effect is assumed for the nanopillars in this work, the reduced PL signal would not be observable in our spectroscopy system.

In summary, the fabrication of uniform optically active InGaAs triangular lattice QD arrays has been demonstrated using NSL combined with an O₂ plasma RIE resizing process and a Br-IBAE vertical dry etch. Low temperature PL data showed energy blueshifts of spectral peak as large as 11 meV from arrays of 170 nm diameter InGaAs QDs. The fabricated structures were modeled using COMSOL, and the resulting model is in agreement with our experimental results with the inclusion of a 70 nm thick etch-damaged dead layer at the perimeter of the nanopillar. We also demonstrated the ability to additionally blueshift of the QD PL spectra by means of an InGaAs-selective wet etch. The uniformity and optical quality of the nanostructure arrays demonstrate an inexpensive enabling technique for the fabrication of 3D nanophotonic and nanoelectronic devices based on the InGaAlAs materials system.

The authors would like to thank the Harvard Center for Nanoscale Systems (CNS) for the use of their Nexx Cirrus 150 RIE system. This work was partially supported by Raytheon Co. and the (U.S.) Air Force Office of Scientific Research (Grant No. FA9550-5-1-6314).

- ¹A. Scherer and H. G. Craighead, *Appl. Phys. Lett.* **49**, 1284 (1986).
- ²J. Christen, M. Krahl, and D. Bimberg, *Superlattices Microstruct.* **7**, 1 (1990).
- ³D. Leonard, M. Krishnamurthy, C. M. Reaves, S. P. Denbars, and P. M. Petroff, *Appl. Phys. Lett.* **63**, 3203 (1993).
- ⁴A. Madhukar, Q. Xie, P. Chen, and A. Konkar, *Appl. Phys. Lett.* **64**, 2727 (1994).
- ⁵J. Ro, S. Kim, and E. Lee, *J. Cryst. Growth* **188**, 377 (1998).
- ⁶D. Bimberg, M. Grundmann, F. Heinrichsdorff, N. N. Ledentsov, V. M. Ustinov, A. E. Zhukov, A. R. Kovsh, M. V. Maximov, Y. M. Shernyakov, B. V. Volovik, A. F. Tsatsul'nikov, P. S. Kop'ev, and Z. I. Alferov, *Thin Solid Films* **367**, 235 (2000).
- ⁷C. Reese, C. Becher, A. Imamoglu, E. Hu, B. D. Gerardot, and P. M. Petroff, *Appl. Phys. Lett.* **78**, 2279 (2001).
- ⁸H. C. Liu, M. Gao, J. McCaffrey, Z. R. Wasilewski, and S. Fafard, *Appl. Phys. Lett.* **78**, 79 (2001).
- ⁹S. Tsuboi and K. Suzuki, *J. Vac. Sci. Technol. B* **11**, 2994 (1993).
- ¹⁰H. G. Craighead, *J. Appl. Phys.* **55**, 4430 (1984).
- ¹¹M. Qi and H. I. Smith, *J. Vac. Sci. Technol. B* **20**, 2991 (2002).
- ¹²K. Arshak and M. Mihov, *J. Optoelectron. Adv. Mater.* **7**, 193 (2005).
- ¹³H. W. Deckman and J. H. Dunsmuir, *Appl. Phys. Lett.* **41**, 377 (1982).
- ¹⁴M. Imada, S. Noda, A. Chutinan, T. Tokuda, M. Murata, and G. Sasaki, *Appl. Phys. Lett.* **75**, 316 (1999).
- ¹⁵A. Bezryadin, C. Dekker, and G. Schmid, *Appl. Phys. Lett.* **71**, 1273 (1997).
- ¹⁶L. L. Chan, P. Y. Li, D. Puff, and B. T. Cunningham, *Sens. Actuators B* **120**, 392 (2007).
- ¹⁷M. Duval Malinsky, K. Lance Kelly, G. C. Schatz, and R. P. Van Duyne, *J. Phys. Chem. B* **105**, 2343 (2001).
- ¹⁸X. Qian, J. Li, and W. D. Goodhue, *Mater. Res. Soc. Symp. Proc.* **1059**, 1059-KK11-10 (Materials Research Society, Pittsburgh, 2008).
- ¹⁹W. D. Goodhue, Y. Royter, D. E. Mull, S. S. Choi, and C. G. Fonstad, *J. Electron. Mater.* **28**, 364 (1999).
- ²⁰R. Steffen, J. Oshinowo, T. Koch, and A. Forchel, *J. Vac. Sci. Technol. B* **13**, 2888 (1995).
- ²¹L. Chu, M. Arzberger, G. Bohm, and G. Abstreiter, *J. Appl. Phys.* **85**, 2355 (1999).
- ²²R. Steffen, Th. Koch, J. Oshinowo, F. Faller, and A. Forchel, *Appl. Phys. Lett.* **68**, 223 (1996).
- ²³B. E. Maile, A. Forchel, R. Germann, A. Menschig, H. P. Meier, and D. Gruetzmacher, *J. Vac. Sci. Technol. B* **6**, 2308 (1988).
- ²⁴W. E. Spicer, I. Lindau, P. Skeath, C. Y. Su, and P. Chye, *Phys. Rev. Lett.* **44**, 420 (1980).